


H. KATAYAMA-YOSHIDA 
K. SATO
H. KIZAKI
H. FUNASHIMA
I. HAMADA
T. FUKUSHIMA
V.A. DINH
M. TOYODA

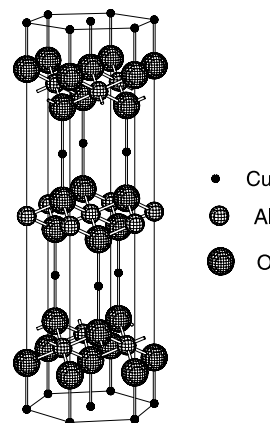
Ab initio materials design for transparent-conducting-oxide-based new-functional materials

Department of Computational Nano-materials Design and Department of Condensed Matter Physics, The Institute of Scientific and Industrial Research, Osaka University, 8-1 Mihogaoka, Ibaraki, Osaka 567-0047, Japan

Received: 16 October 2006/Accepted: 5 April 2007
Published online: 25 May 2007 • © Springer-Verlag 2007

ABSTRACT Based upon ab initio electronic structure calculations for delafossite CuAlO_2 and ZnO , we report on the design of new-functional materials for transparent conducting oxides (TCO), such as (i) low-resistive p-type ZnO and CuAlO_2 by co-doping, (ii) high-efficiency thermoelectric power in CuAlO_2 ($ZT > 3$) by p-type doping, (iii) half-metallic ferromagnetism in transition-metal-impurity doped CuAlO_2 and ZnO -based diluted magnetic semiconductors, and (iv) CaO , MgO , SrO and BaO based DMS without transition metal impurities. We also discuss the implementation of the self-interaction correction to our materials design method.

PACS 61.72.Bb; 61.72.Jj; 71.15.Mb; 72.15.Jf; 82.75.-d



CuAlO_2 (Delafossite)

FIGURE 1 Crystal structure of delafossite CuAlO_2

1 Introduction

Based upon ab-initio electronic structure calculations, we have proposed the material design of new CuAlO_2 - and ZnO -based functional materials, such as transparent conducting oxides (TCO) [1–5], dilute magnetic semiconductors (DMS) [6–16], high- T_c superconductors [17], high efficiency thermoelectric materials [18] and so on. In this paper, we review some of our recent progress mainly focusing on CuAlO_2 and ZnO .

CuAlO_2 has a Delafossite structure. The Delafossite (CuFeO_2) was discovered by C. Friedel in 1873 and named by him in the honor of G. Delafosse [19]. The Delafossite structure is a rhombohedral structure with four atoms per unit cell. The conventional hexagonal unit cell of CuAlO_2 is shown Fig. 1.

After the discovery of p-type conductivity in the Delafossite CuAlO_2 without any intentional doping [20], the Delafossite CuAlO_2 was highlighted as a low-resistive p-type TCOs. It is well known that for wide gap semiconductors such as ZnO and GaN , n-type doping is easy while p-type doping is prohibitively difficult. Nowadays n-type TCOs such as ZnO , In_2O_3 , SnO_2 are used as transparent electrodes. However, monopolarity of these materials restricts their practical applications. Thus, CuAlO_2 is a potential material for application

to efficient photovoltaic solar cells by using a p–n junction combined with an n-type TCO such as ZnO or indium tin oxide (ITO).

In the following, we discuss a thermal non-equilibrium valence control method upon co-doping in CuAlO_2 and ZnO for realizing low resistive p-type TCO [1–5, 17]. Then, we study the thermoelectric properties of CuAlO_2 and demonstrate the high Seebeck coefficient of CuAlO_2 [18]. We also propose CuAlO_2 - and ZnO -based dilute magnetic semiconductors (DMS) for semiconductor spintronics [6–12]. Our material designs for TCO-based DMS are developed for the design of exotic DMS such as CaO , MgO , SrO and BaO based DMS without transition metal impurities [13–15]. Finally, we discuss the effect of the self interaction correction to our materials design [16].

2 Design of valence control method

2.1 Native defects in CuAlO_2

The carrier density of p-type CuAlO_2 is $1.3 \times 10^{17} \text{ cm}^{-3}$ and resistivity is $11 \Omega \text{ cm}$, which is much higher than that of ITO ($\sim 10^{-5} \Omega \text{ cm}$). Therefore for practical applications based on TCOs, it is necessary to develop an efficient doping method to fabricate a low-resistive p-type CuAlO_2 . For this purpose, we must first discuss the mechanism of p-type conductivity of CuAlO_2 by performing ab-initio cal-

culations of the electronic structure and the energy of native defects in CuAlO_2 .

Calculations were performed within the local density approximation (LDA) to density functional theory using the Ceperley–Alder exchange–correlation energy and potential, as parameterized by Perdew and Zunger. We used ultrasoft pseudopotential to describe electron–ion interactions and a plane wave basis set to expand the wave functions. To model the isolated defects we used a $2 \times 2 \times 2$ rhombohedral supercell, which contains eight rhombohedral primitive unit cells. Atomic positions were fully relaxed without any symmetry constraints at the theoretical lattice parameters. For charge defects, a jellium background was used to keep the whole system charge neutral. We also calculated the formation energy of some selected defects using a larger supercell and found that the change in the calculated formation energy is up to 1 eV. Thus, the error in the transition energy is non-negligible. However, the relative stability of the formation energy and relative positions of the transition levels are unchanged, thus our conclusion remains unchanged.

Following the notation of [21], the formation energy $\Delta H(\alpha, q)$ of a defect α in a charge state q was calculated. Calculation details can be found in [4]. It is found that $\Delta H(\text{V}_{\text{Cu}}^-)$ is always negative within the energy gap, that means, V_{Cu}^- will form spontaneously under this condition (Cu-poor and oxygen rich). Moreover the position of the defect transition level $\varepsilon(\text{V}_{\text{Cu}}^-/\text{V}_{\text{Cu}}^-) = E_{\text{VBM}} - 0.44 \text{ eV}$, so V_{Cu}^- does not induce energy levels within the energy gap. The transition level below the valence band maximum (VBM) was also found in previous work. The origin of the negative transition level is the anti-bonding character of the Cu- d -O- p bands at the VBM. Also, the atomic relaxation is quite small because of the weak bonding of the O–Cu–O dumbbell due to this p - d anti-bonding character.

When E_{F} is at the midgap, $\Delta H(\text{O}_i)$ becomes negative and will form spontaneously as V_{Cu}^- . However the defect transition energies are $\varepsilon(\text{O}_i^-/\text{O}_i^-) = E_{\text{VBM}} + 0.70 \text{ eV}$ and $\varepsilon(\text{O}_i^-/\text{O}_i^{2-}) = 1.38 \text{ eV}$, being deep levels. Oxygen interstitial will form a localized state and will not contribute to good conductivity. As E_{F} moves toward the conduction band minimum (CBM), the formation energy of oxygen antisites O_{Cu} decreases. Over the whole range of the Fermi energy, acceptor type defects have low formation energy and donor type defects such as copper antisite Cu_{O} , oxygen vacancy V_{O} , and copper interstitial Cu_i hardly occur, because their formation energy is high.

However, under the copper-rich and oxygen-poor limit, the formation energies of acceptors increase and those of donors decrease. $\Delta H(\text{V}_{\text{Cu}})$ becomes positive near the VBM. However, $\Delta H(\text{V}_{\text{Cu}}^-)$ is still low and becomes negative above the midgap, and thus spontaneously forms. Over the range of the chemical potentials and the Fermi energy, the formation energies of copper vacancy and oxygen interstitial are low compared with other acceptor- and donor type defects. Our results indicate that the controlling of copper and oxygen pressure is very important to fabricate (low-resistive) CuAlO_2 and that copper vacancy also plays an important role in the p-type conductivity. For example, the copper-vacancy doping by reducing the copper partial pressure could be an efficient doping method [5, 17].

2.2 Thermal non-equilibrium valence control upon codoping

In the thermal equilibrium crystal growth condition, it is very difficult to realize both the low-resistive p- and n-type materials in the wide-gap semiconductors (this so called “uni-polarity”), such as oxides and nitrides, due to (i) the self-compensation, (ii) the deep acceptor (or donor) level around 500 meV by small dielectric constant, and (iii) the low solubility (high formation energy) of the dopants around 10^{16} cm^{-3} . In the thermal equilibrium condition, we cannot avoid the uni-polarity where we can go only one way to the p-type or n-type. For example, n-type doping by Ga, In or Al donor-impurity is very easy in ZnO and we can fabricate metallic transparent n-type conductors, however, p-type doping by N, As or Sb acceptor-impurities is extremely difficult in ZnO and usually self-compensation occurs and becomes insulating. Based on the tremendous experimental, theoretical and ab-initio calculations in the last 20th-century, it becomes clear that we cannot fabricate both p- and n-type wide-gap semiconductors in thermal equilibrium crystal growth conditions. This means that, if we stand by the thermal equilibrium condition, we have no excellence, no leadership and no innovation for the valence control to go beyond the uni-polarity problem in wide-gap semiconductors. Therefore, mostly in Japan, crystal growers gave up using the thermal equilibrium crystal growth method and shifted to the thermal non-equilibrium crystal growth method for high concentration doping of acceptors and donors by using MBE, MOCVD and MOVPE.

In order to overcome the above “uni-polarity” problem in wide-gap semiconductors under the thermal non-equilibrium crystal growth condition, we propose the new valence control method of reactive co-doping in wide-gap semiconductors such as ZnO, CaO, GaN, AlN or diamond. Since the acceptor (or donor) has low solubility with high formation energy, the effective chemical interaction between the acceptor and acceptor (or donor and donor) is attractive. Therefore, the aggregation of the acceptors (or donors) usually occurs upon high concentration of the doping. If we co-dope the acceptors and donors (1 : 1) in the same concentration at the same time, we can make inhomogeneous doping in the thermal non-equilibrium condition (see Fig. 2a). We have no carriers due to the perfect compensation between the acceptor and donor (see Fig. 2c), however the local band gap at the aggregated area becomes smaller than the low concentration area of impurities due to the inhomogeneous distribution of the acceptor and donor impurities. Then, we can try high concentration co-doping of acceptors and donors at the same time as we create an imbalance in the doping vapor pressures (2 : 1) in the thermal non-equilibrium crystal growth methods such as MBE, MOCVD or MOVPE. We can enhance the nano-scale size of the inhomogeneous distribution of acceptor–donor–acceptor (or donor–acceptor–donor) complexes (see Fig. 2b) and reduce the activation energy of acceptor (or donor) one order of magnitude, for example, from 500 meV to 50 meV (see Fig. 2d). We propose the universal valence control method, the so called reactive “co-doping method”, in which we can use the merits of low solubility and high activation energy (deep impurity) of the acceptor (or donor) in the wide-gap semiconductors in an efficient

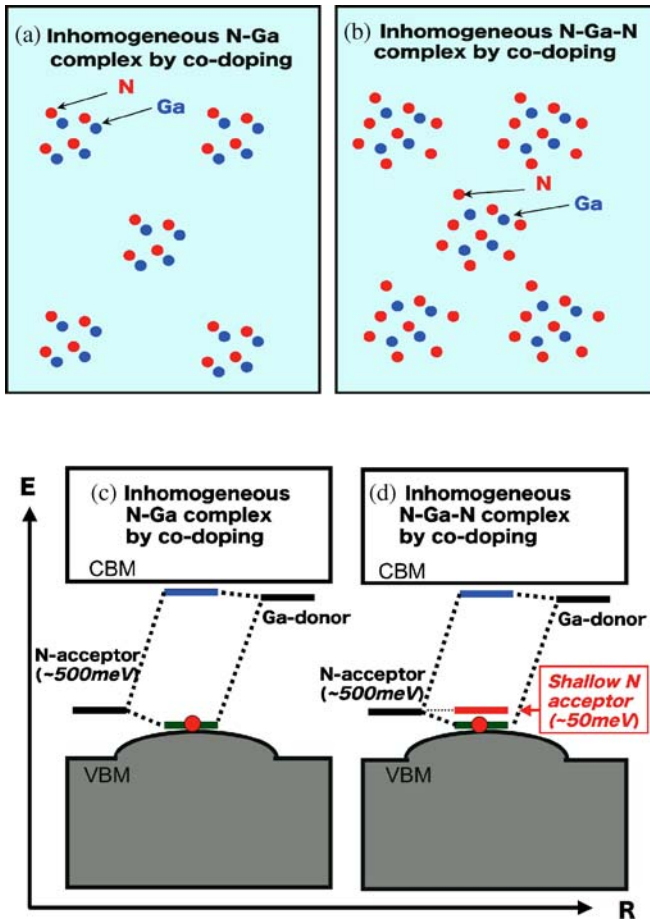


FIGURE 2 Co-doping method of acceptor (N) and donor (Ga) in ZnO

way by using the thermal non-equilibrium crystal growth technique.

The process of the co-doping method for the universal valence control method is as follows.

- (i) We should choose the uni-polarity system of the wide-gap semiconductors with low solubility and deep-acceptor (or donor) level in the band gap.
- (ii) Using the thermal non-equilibrium crystal growth methods such as MBE, MOCVD, or MOVPE, we should co-dope the acceptors and donors with high concentrations (10^{20} – 10^{21} cm^{-3}) at the same time as we create an imbalance in the doping vapor pressures (2 : 1) [see Fig. 2b].
- (iii) We should make the acceptor–donor–acceptor (or donor–acceptor–donor) complexes and the inhomogeneous distribution of these complexes in the nano-meter-scale size using the spinodal nano-decomposition by controlling the crystal growth speed, the partial vapor pressure of the dopant and the temperature under the thermal non-equilibrium conditions [see Fig. 2b].
- (iv) We should control the spatial distribution of the band-gap by the above modulation co-doping in the spinodal nano-decomposition [see Fig. 2d].

Figure 3 depicts the comparison of the partial N-2p density of states between the N mono-doping and N–Ga–N co-doping using the super-cell calculation for different

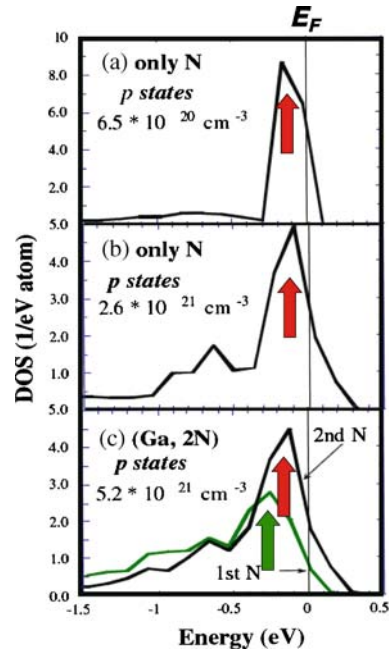


FIGURE 3 Calculated partial N-2p density of states (DOS) at the N-site in ZnO [1–3]

N-acceptor concentrations. The partial N-2p density of states (DOS) at the different N-sites (1st and 2nd nearest neighbor N-site measured from the co-doped Ga-site) in the N–Ga–N co-doping case indicate clearly that the Ga–N (1st nearest neighbor atom) bond forms the bonding and compensated state by lowering the energy from the isolated N-acceptor level. Therefore, we can expect that the first excited state from the highest occupied states in the VBM to the unoccupied acceptor level correspond to the transition from the blue arrow to the red arrow in Fig. 2c. These results indicate that the inhomogeneous distribution of N–Ga–N complexes caused by spinodal nano-decomposition of N–Ga–N high concentration and N–Ga–N poor concentration regions, creates the spatially (R) different distribution of the band-gap in the co-doped ZnO with the higher concentration ($\sim 10^{21}$ cm^{-3}).

We applied our new valence control method of co-doping for the fabrication of low-resistivity p-type GaN, AlN, ZnSe, and ZnO, which is proposed by ab-initio electronic structural calculations [1–3]. We propose the following codoping method (using both n- and p-type reactive dopants at the same time) to fabricate a low-resistivity p-type semiconductors; (1) GaN: [$\text{Si}_{\text{Ga}} + 2\text{Mg}_{\text{Ga}}$ (or Be_{Ga}), $\text{H} + 2\text{Mg}_{\text{Ga}}$ (or Be_{Ga}), and $\text{O}_{\text{N}} + 2\text{Mg}_{\text{Ga}}$ (or Be_{Ga})], (2) AlN: [$\text{O}_{\text{N}} + 2\text{C}_{\text{N}}$], (3) ZnO: [$\text{Ga}_{\text{Zn}} + 2\text{NO}$, $\text{Al}_{\text{Zn}} + 2\text{NO}$, and $\text{In}_{\text{Zn}} + 2\text{NO}$], and (4) ZnSe: [$\text{In}_{\text{Zn}} + 2\text{N}_{\text{Se}}$, $\text{Cl}_{\text{Se}} + 2\text{N}_{\text{Se}}$, $2\text{Li}_{\text{Zn}} + \text{Cl}_{\text{Se}}$ (or I_{Se}), and $\text{Te}_{\text{Se}} + 2\text{N}_{\text{Se}}$]. We compared our predictions of co-doping with the recent successful co-doping experiments for the fabrication of the low-resistivity p-type wide band-gap semiconductors.

3 Design of efficient thermoelectric materials

In 1950s, Ioffe found that doped semiconductor was one of the best thermoelectric materials [22]. After that,

the thermoelectric properties of semiconductors, semimetals and alloys were studied intensively in the 1960s–1970s. In this section, we discuss the thermoelectric properties of CuAlO_2 based on ab-initio electronic structural calculations [18].

We have calculated electric structures by using the full-potential linearized augmented plane wave (FLAPW) method within the LDA. The KANSAI99 FLAPW package developed by H. Harima and A. Yanase was used for the present calculations. To calculate thermoelectric properties such as electric conductivity σ and the Seebeck coefficient S , we used the Mott and Jones Formula [23]. In this study, carrier doping effects were treated by the rigid-band approximation. Moreover, we suppose that the relaxation time τ is constant, because we consider that the impurity scattering is the dominant cause of electron scattering.

As shown in Fig. 1, the crystal structure of CuAlO_2 consists of the Cu–O–Cu dumbbell and the AlO_2 octahedron. Accordingly, we can distinguish characteristic features of the density of states, namely, that the DOS shows the bands formed by the p – d hybridization between O and Cu. These bands are inserted in the wide band gap (6 eV) originating from the AlO_2 octahedron. The total bandwidth of these p – d hybridized states is 4 eV. These states consist of anti-bonding ($3d(3z^2 - r^2)$, $3d(yz)$, $3d(zx)$) nonbonding ($3d(x^2 - y^2)$, $3d(xy)$) and bonding ($3d(3z^2 - r^2)$, $3d(yz)$, $3d(zx)$) states, thus the states at the valence band maximum shows an anti-bonding $3d(3z^2 - r^2)$ character.

Calculated DOS shows a sudden increase at the valence band maximum reflecting the flat band feature around the valence band maximum. According to the formula by Mott and Jones [23], the Seebeck coefficient is proportional to the energy differential of the density of states. Thus we expect a large Seebeck efficiency. Actually, the calculated thermoelectric property shown in Fig. 4a shows a large Seebeck coefficient around the valence band top where the energy differential of the density of states is large. As a result, the

p -type doping into this material leads to a large power factor (Fig. 4b).

4 Materials design for semiconductor spintronics

In this section, we discuss the magnetism in dilute magnetic semiconductors (DMS) from first-principles [6–16]. For the electronic structure calculations, we use the Korringa–Kohn–Rostoker coherent-potential-approximation method and a local density approximation (KKR-CPA-LDA) [24] package (MACHIKANEYAMA2002 [25]) developed by Akai. The DMS system is a disordered system. For example, in ZnO-based DMS Zn atoms are randomly substituted by transition metal (TM) impurities. In the present calculations, this substitutional disorder is treated by using the KKR-CPA. In the KKR-CPA, the effective medium, which describes the configuration averaged disordered system, is calculated self-consistently within the single site approximation.

In the framework of the KKR-CPA method, the concept of disordered local moment (DLM) state is conveniently used to describe the paramagnetic state at finite temperature [24]. It is known that the DLM state describes well, the paramagnetic state of a ferromagnet above T_C and in the mean field approximation (MFA) we can estimate T_C from total energy difference between the DLM and the ferromagnetic state [26]. This approach was used for a systematic study of the origin of the ferromagnetism in III–V DMS [26, 27]. We use this method for the present materials design of TCO-based DMS. Before the discussion on the materials design for semiconductor spintronics, we explain the mechanism of the ferromagnetism in DMS.

4.1 Magnetic interactions in DMS and general chemical trends

As shown later, the characteristic features of the density of states (DOS) of the ZnO-based DMS are sketched

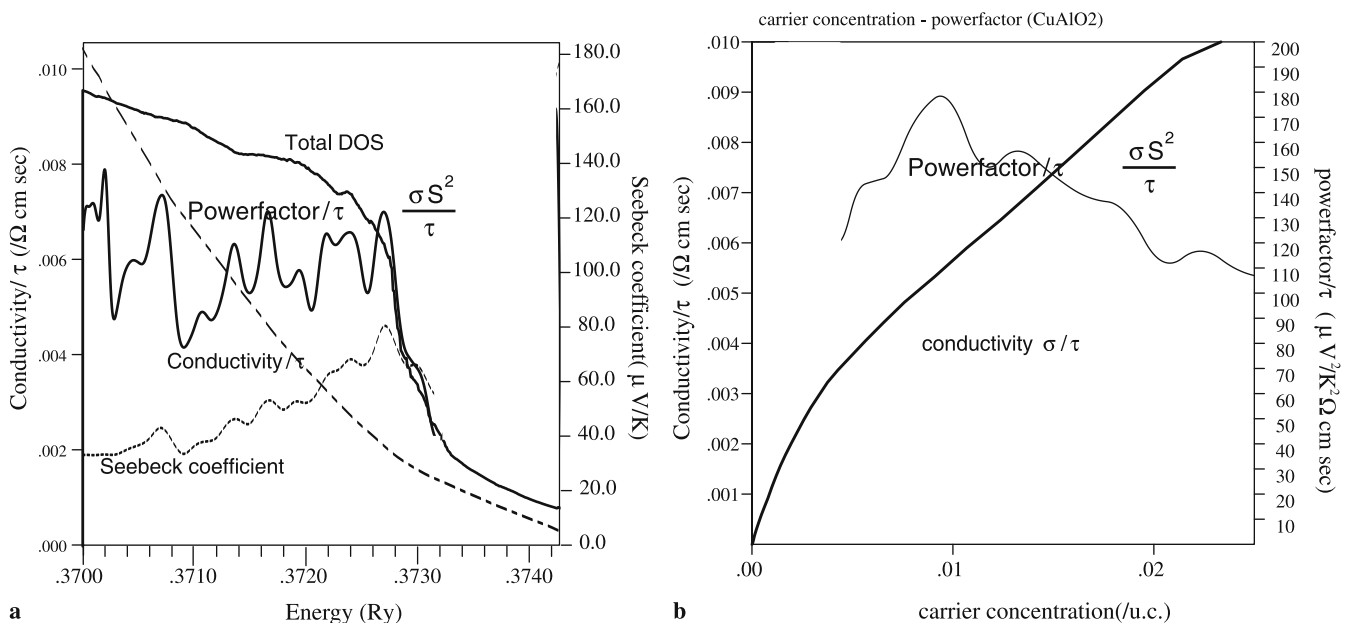


FIGURE 4 Calculated thermoelectric properties of CuAlO_2 as a function of (a) E_F and (b) hole concentration

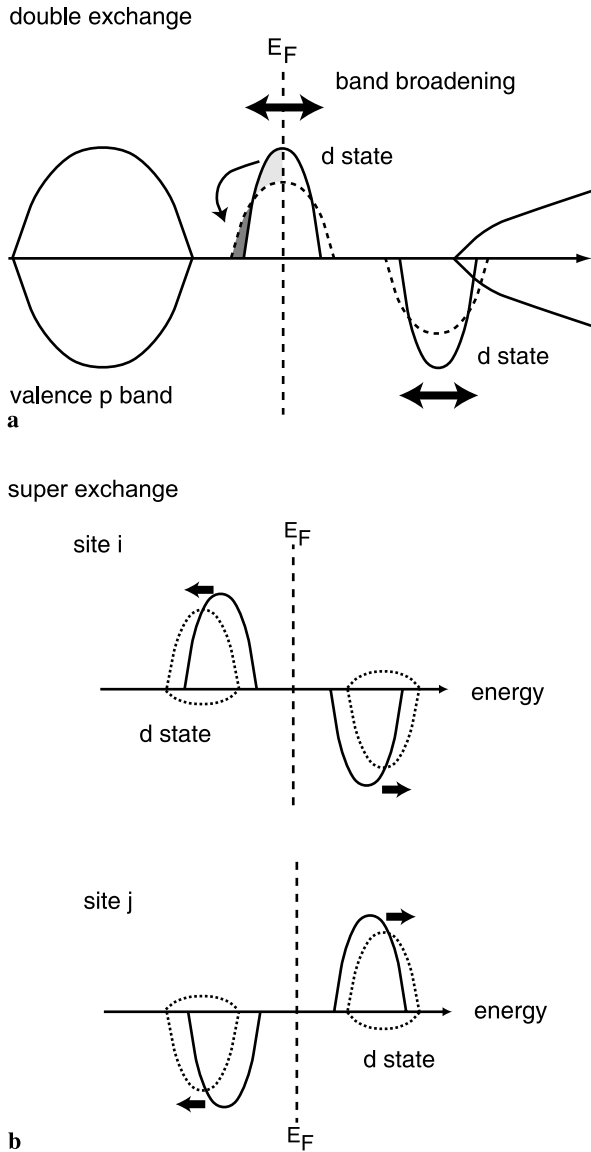


FIGURE 5 Magnetic exchange interactions in DMS; (a) double exchange, (b) super exchange

in Fig. 5a. The Fermi energy (E_F) lies in the majority impurity band. The important energy gain arises from the broadening of the impurity band with increasing concentration c . If we increase the concentration from a lower value, with the DOS given by the full line, to a larger value corresponding to the broader DOS as given by the dashed line, we transfer the DOS-weight from around E_F to lower energies, leading to an energy gain, which, as we will show, stabilizes the ferromagnetic state. This energy gain is proportional to the bandwidth W of the impurity band, which scales as the square root of the concentration. The energy gain due to band broadening is known as Zener's double exchange [27, 28].

Let us now consider the stability of the DLM state as compared to the ferromagnetic one. In the CPA-description of the DLM state, for a given TM atom, 50% of the neighboring TM atoms have a moment being parallel aligned to the central moment, and 50% are anti-ferromagnetically aligned [29]. The parallel aligned pairs lead, as in the ferromagnetic case, to

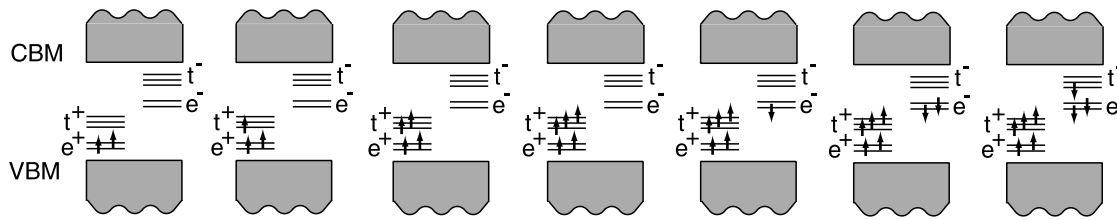
a broadened impurity band, but with a reduced band width scaling as $\sqrt{c/2}$, since only 50% of the pairs are aligned parallel. Therefore, in total the double exchange due to band broadening always favors the ferromagnetic configuration.

The 50% anti-ferromagnetically aligned pairs gain energy by super-exchange [27, 30, 31]. The density of states in the gap of two Mn impurities with anti-parallel aligned moments is schematically shown in Fig. 5b. Note that the minority and majority peaks are exchanged for the two atoms. Since the wave functions with the same spin directions hybridize with each other, covalent bonding and anti-bonding hybrids are formed. From the energetic point of view it is important that the lower bonding states are shifted to lower energies, while the higher anti-bonding states are shifted to higher energies. Thus energy is gained by super-exchange, if the Fermi energy is located between the two peaks or in the peaks, however not, if E_F is below or above both peaks. As can be shown, the energy gain is given by ct^2/IM , where t is the effective hopping matrix element and IM is the exchange splitting, given by the exchange integral I times the local moment M . It is linear in c , since the effects of several anti-parallel aligned neighbors on the central atom superimpose on each other.

Thus in the case of impurity bands in the gap, double exchange favors the ferromagnetic configuration and always wins, if the Fermi energy lies (well) in the band. Then the energy gain due to double exchange, scaling as $\sqrt{c}|t|$, is always larger than the energy gain due to super exchange, scaling like $c|t|^2/IM$. However if the Fermi energy lies between the two bands or lies close to the band edges, super exchange wins by stabilizing the disordered local moment state. Thus the system (Zn,Cr)O is expected to be a ferromagnet, while (Zn,Mn)O should be a DLM system since the impurity band is completely filled. For the same reason, in the III-V compounds Mn impurities should favor the ferromagnetic state, while Fe impurities favor the DLM state.

According to general discussions on the electronic structure of TM impurity in semiconductors [32], fivefold degenerated d -states of TM impurity are split into doubly degenerated $d\gamma$ -states and threefold degenerated $d\varepsilon$ -states in the tetrahedral coordination. Two $d\gamma$ -states have the symmetry of $3z^2 - r^2$ and $x^2 - y^2$. Three $d\varepsilon$ -states have the symmetry of xy , yz and zx . The wave functions of these $d\varepsilon$ -states are extended to anions, therefore, $d\varepsilon$ -states hybridize well with O-2p states which make the host valence band, so that bonding states (t^b) and anti-bonding counterparts (t^a) are created. However, the wave functions of $d\gamma$ -states are extended to the interstitial region, therefore, the hybridization of $d\gamma$ -states with the host valence band is weak and $d\gamma$ -states remain as non-bonding states (e).

In ZnO-based DMS, the magnetism is determined by the competition between ferromagnetic double exchange and anti-ferromagnetic super exchange. In order to stabilize the ferromagnetism efficiently, there should be electrons that have a considerable itinerant character. As a natural consequence, it is suggested that the ferromagnetic state is stable when delocalized t^a -states are partially occupied. From this comes a simple rule by which we propose to explain the magnetism of DMSs [10]. Provided that TM has a 2+ or 3+ formal charge state in II-VI or III-V, respectively, their 3d-electron configurations are expected to be those shown in Fig. 6. In the same



II-VI	Ti ²⁺ (3d ²)	V ²⁺ (3d ³)	Cr ²⁺ (3d ⁴)	Mn ²⁺ (3d ⁵)	Fe ²⁺ (3d ⁶)	Co ²⁺ (3d ⁷)	Ni ²⁺ (3d ⁸)
III-V	V ³⁺ (3d ²)	Cr ³⁺ (3d ³)	Mn ³⁺ (3d ⁴)	Fe ³⁺ (3d ⁵)	Co ³⁺ (3d ⁶)	Ni ³⁺ (3d ⁷)	Cu ³⁺ (3d ⁸)
Double exchange	—	FM	FM	—	WFM	—	FM
Super exchange	FM	AFM	AFM	AFM	AFM	FM	AFM

FIGURE 6 Electron configuration of magnetic impurities in DMS and chemical trend of magnetism in III-V and II-VI DMS. FM (ferromagnetic), AF (anti-ferromagnetic) and WFM (weakly ferromagnetic) indicate the magnetic interaction between TM impurities

figure, predicted magnetic states by the rule are also shown. This prediction should be confirmed by the ab-initio materials design in the later section.

4.2 Materials design of ZnO-based dilute magnetic semiconductors

In Fig. 7, we have calculated the total energy difference per one formula unit between the ferromagnetic state and the DLM state as is shown for V-, Cr-, Mn-, Fe-, Co- and Ni-doped ZnO and ZnTe. There is no additive impurity such as carrier dopants other than TM impurities. In Fig. 7, the positive energy difference indicates that the ferromagnetic state is more stable than the DLM state. As shown in the figure, for Mn-doped ZnO and ZnTe, the DLM state is most stable in all of the TM impurities. For V- and Cr-doped ZnO and ZnTe, the ferromagnetic states are more stable than the DLM states. For Fe-, Co- and Ni-doped ZnTe, the ferromagnetic states are going to be stabilized by increasing the atomic number of TM, however the DLM states are still stable. However, the ferromagnetic states are stable for Fe-, Co- and Ni-doped ZnO-based DMSs. At this point, ZnO-based DMSs are distinguished from the others [6–10].

Energy difference of 1.36 mRy obtained for 25% V-doped ZnO is very large and corresponds to T_C of 570 K within the mean field approximation (MFA). If the MFA is reasonably good, high- T_C is suggested for V-, Cr-, Fe-, Co- and Ni-doped ZnO, and V- and Cr-doped ZnTe. However, recently it was pointed out that due to the lack of magnetic percolation, high- T_C , it is generally difficult to realize in DMS for low concentrations [33–35].

Recently, TM-doped ZnO thin films have been systematically synthesized owing to the successful construction of combinatorial laser MBE equipment [36], and our material design of ZnO-based DMSs has been of much interest for experimenters [37]. One of the most interesting points for an application is that ZnO-based DMSs are transparent with visible light [36]. Taking our materials design into account, it is suggested that ZnO-based DMSs will be transparent ferromagnets, which should encourage the inventing of new devices making use of the magneto-optical effects. From this point of view, some experiments have been performed to investigate the magnetism of ZnO-based DMSs, and ferromagnetic behavior was reported in (Zn,V)O [38], (Zn,Co)O [39] and (Zn,Ni)O [40] above room temperature. However, the ferromagnetic interaction was not detected in the magneto-optical

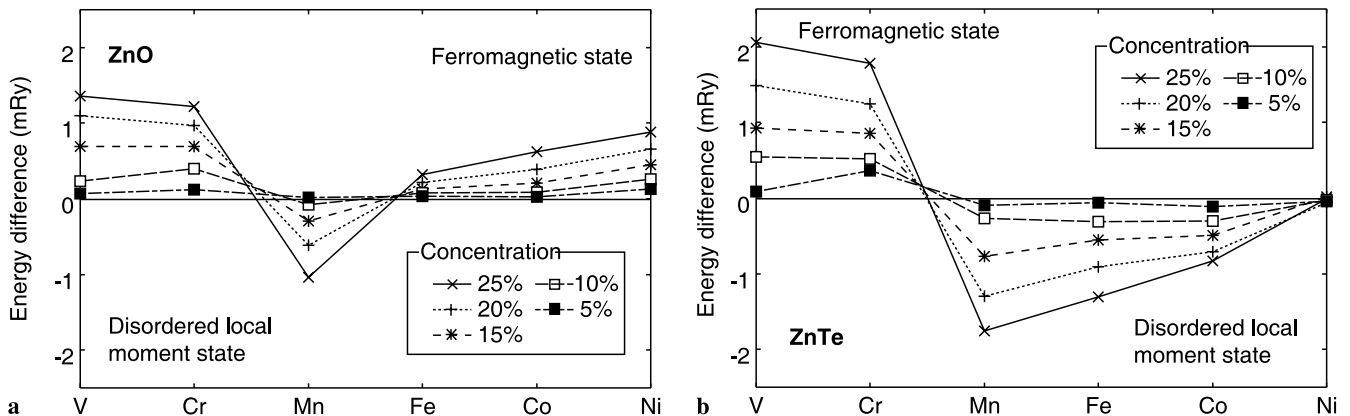


FIGURE 7 Stability of the ferromagnetic state in (a) ZnO-based DMS and (b) ZnTe-based DMS

effects [41]. More experimental efforts are needed to confirm the ferromagnetism in ZnO-based DMSs and to apply them to practical applications. In ZnTe-DMS, the ferromagnetism of (Zn,Cr)Te is well established by the experiments [42, 43].

In Fig. 8, total density of states (DOS) per unit cell and partial DOS of 3d-states per TM atom at the TM site are shown for the ferromagnetic state of ZnO-based DMS. TM atoms are doped up to 5% in each case. The horizontal axis represents energy relative to the Fermi energy. The host valence band consists of two parts. One is the low-lying Zn-3d band which appears at approximately 0.5 Ry below E_F as a peak whose width is 0.15 Ry. The other is a broad O-2p band which is distributed from -0.4 Ry to -0.2 Ry. Between the valence band and the conduction band, which consists of Zn-4s states, there are impurity-3d bands. These impurity bands show a large exchange splitting, and they are gradually occupied on increasing the atomic number of the impurity. As the exchange splitting is larger than the crystal field splitting as shown in Fig. 8, all TMs are in high spin states. In particular, the half-metallic DOS are realized in V-, Cr-, Fe-, Co- and Ni-doped ZnO. The half-metallic DOS means that the DOS is metallic for up spin states and insulating for down spin states, or vice versa. This kind of asymmetry in the DOS at E_F is shown in the other II-VI based DMSs, and it is proposed that these II-VI compound based DMSs are useful to realize spintronics devices such as a spin injection device and a spin-polarized FET and so on.

In Fig. 8c, it is shown that the Mn impurity has a d^5 electron configuration due to the substitution of Zn^{2+} by Mn^{2+} . In this case, it is suggested that the anti-ferromagnetic superexchange interaction between Mn ions stabilize the DLM state. However, V^{2+} , Cr^{2+} , Fe^{2+} , Co^{2+} and Ni^{2+} have d^3 , d^4 , d^6 , d^7 and d^8 electronic configurations, respectively, therefore, 3d-band of up-spin states or down-spin states are not fully occupied and the ferromagnetic state is stabilized due

to the ferromagnetic double exchange. These calculation results correspond well to our prediction in Sect. 4.1 based on the double-exchange vs. super-exchange model.

4.3 CuAlO₂-based DMS

CuAlO₂ is a transparent semiconductor and has a direct band gap of 3.5 eV and an indirect gap of 1.8 eV. Recently, CuAlO₂ has attracted much attention as a candidate for low-resistive p-type transparent conducting oxide. Moreover, due to its characteristic electronic structure CuAlO₂ is a promising compound for effective thermoelectric materials. In this paper, we explore another potential use of CuAlO₂ and propose a first-principles material design of ferromagnetic DMS based on CuAlO₂ for semiconductor spintronics [12].

In order to obtain the overall chemical trend of the magnetic states of CuAlO₂-DMS, we calculate the total energy difference between the ferromagnetic state and the DLM state of (Cu,TM)AlO₂, where TM = V, Cr, Mn, Fe, Co and Ni, by using the KKR-CPA method in connection with the LDA. It is found that all of the TM impurities show high-spin magnetic states and the ferromagnetic state is stable in Mn-, Fe-, Co- and Ni-doped CuAlO₂. Their calculated electronic structure shows a clear impurity band in the band gap and this means that the ferromagnetism is stabilized due to the double exchange mechanism. All of the ferromagnetic (Cu,TM)-DMS show half-metallic density of states.

4.4 Other oxides for semiconductor spintronics

In this subsection, we discuss the material design based on the other oxides such as SiO₂, CaO, MgO, SrO and BaO. First, we comment on the material design of SiO₂ based DMS. SiO₂ has attracted much attention because of its application potential in ceramic and glass industries, in optical fibers, catalysis and microelectronics. In particular, SiO₂

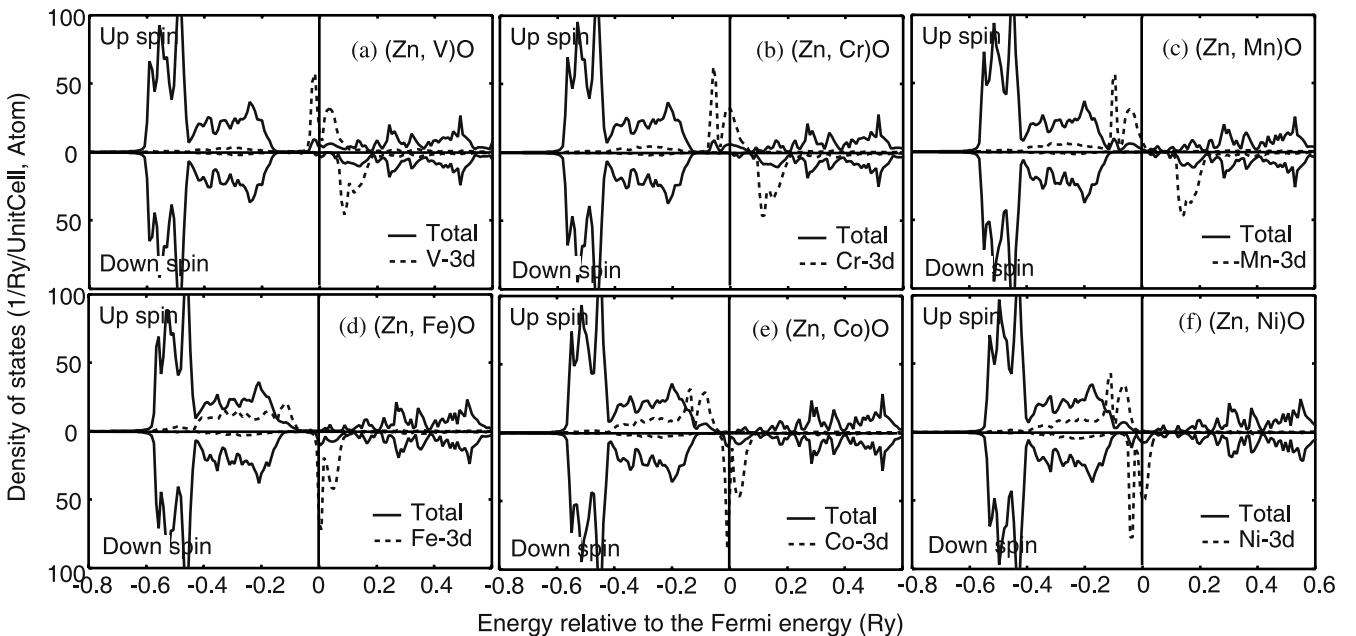


FIGURE 8 Total and partial density of states of ZnO-based DMS in the ferromagnetic state. The concentration of TM impurity is 5%

plays an important role in the Si/SiO₂ interface of Si-based technology. The ab-initio investigation of electronic structures of SiO₂ suggests that this material might be useful for spintronic applications. The α -quartz is the stable phase of SiO₂, and its hexagonal primitive unit cell has three SiO₂ formula units.

To fabricate SiO₂-based DMS, we use V, Cr, Mn and Co to substitute for Si, and to calculate the total energy difference between the ferromagnetic state and the DLM state. Our ab-initio material design shows that all the materials in question are half-metallic. It is found that V has V⁴⁺ (d^1) electron configuration and the Fermi level crosses over the non-bonding states of up spins with 1/2 of the states being occupied. Thus, the ferromagnetic double exchange is dominant to stabilize the ferromagnetism. In the case of Cr doping, Cr has a Cr⁴⁺ (d^2) configuration and the Fermi level lies between non-bonding and anti-bonding states of up spins. In this case, due to the Kanamori–Goodenough rule the super exchange works ferromagnetically and the ferromagnetic state is more stable than the DLM state. In (Si,Mn)O₂ and (Si,Co)O₂, the Fermi levels are located in the impurity band and the double exchange stabilizes the ferromagnetic state [11].

We have applied this material design method to exotic DMS, namely CaO, MgO, SrO and BaO based DMS. So far, we have considered the DMS doped with transition metal impurities. Kenmochi et al. has proposed “deep impurity band engineering” to realize ferromagnetic DMS without transition metal impurities [13, 14]. According to their theory, we can control the band width W and the electron correlation energy U to satisfy Stoners condition ($U > W$). Under this condition, deep impurity bands are formed in the band gap. They argue that by controlling the Fermi level by appropriate carrier doping treatment we can stabilize the ferromagnetic state by using the ferromagnetic double exchange. Along this scenario, they have shown that Nitrogen doped CaO and Carbon doped CaO [13], MgO, SrO and BaO [14] show ferromagnetism with half-metallic DOS.

5 Materials design based on the method beyond the LDA

So far, our material design is based on the electronic calculations within the LDA. It is well known that the LDA underestimates the electron correlation effects and that occupied d -states are systematically predicted at too high energies. Moreover, the LDA underestimates the band gap energy of semiconductors. One major source of these shortcomings of LDA is the presence of self-interaction. We therefore carry out the calculations on ZnO-based DMS by using an LDA with a self interaction correction (SIC). To do so, we implement the SIC to the MACHIKANEYAMA2002 KKR-CPA-LDA package [16]. We employ a pseudo-SIC method as proposed by Filippetti et al. [44].

Calculated DOS of ZnO-based DMS by the SIC-LDA method shows a significant difference from the LDA DOS as shown in Fig. 9. The Zn $3d$ bands, those that are located immediately below the valence band in LDA, show the shift to the lower energy side in the SIC-LDA. As a consequence, the hybridization between the valence band and Zn $3d$ states is significantly reduced resulting in increased gap energy. The calculated impurity bands show large splitting between occupied states and unoccupied states as shown in Fig. 9, resulting in a significant reduction of the d -component at the Fermi energy. The experimental partial density of d states in (Zn,V)O and (Zn,Co)O is reasonably reproduced by the present LDA-SIC calculations. In general, the reduction of d states at the Fermi energy means suppression of ferromagnetic interactions. In principle, similar results were obtained by using the LDA + U method [45]. Systematic calculations for magnetic properties of ZnO-based DMS by using the LDA-SIC are strongly recommended.

This LDA-SIC method for material design was recently applied to the design of ferromagnetic DMS without transition metal impurities. Dinh et al., have succeeded in explain-

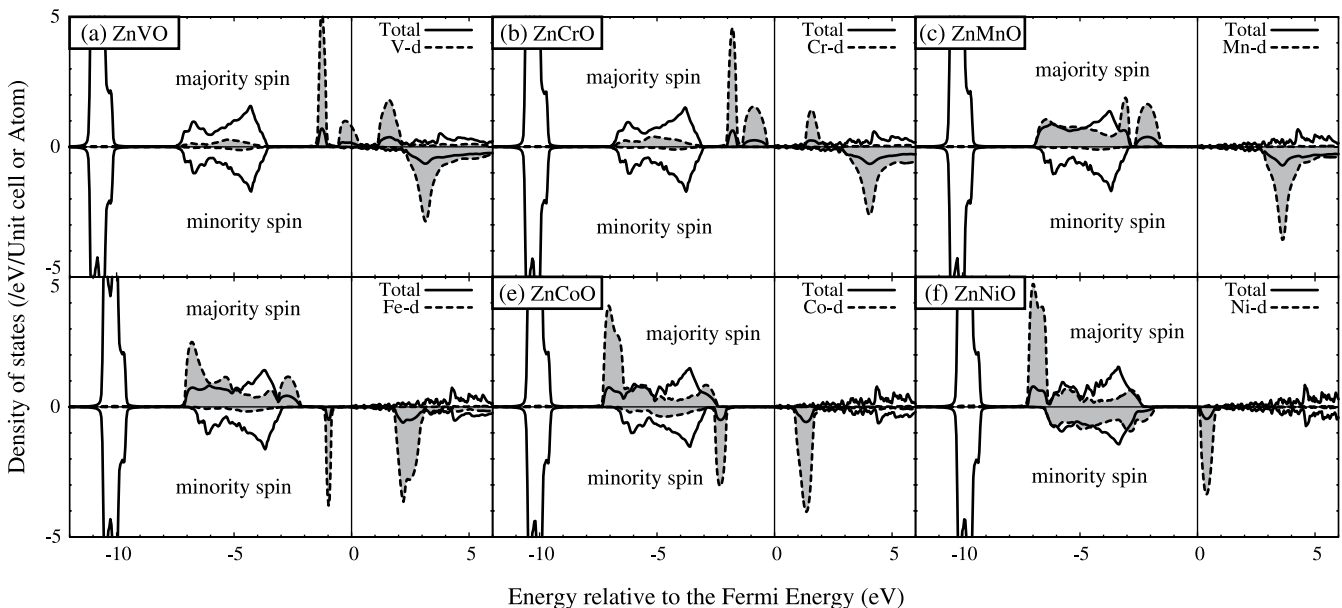


FIGURE 9 Total and partial DOS of ZnO-based DMS in the ferromagnetic state calculated by the SIC-LDA method

ing the origin of the ferromagnetism in C-doped MgO, CaO, SrO and BaO by using the LDA-SIC method [15].

6 Summary

We have discussed some examples of our recent computational materials for the design of new-functional materials for TCOs such as (i) low-resistive p-type ZnO and CuAlO₂ by co-doping, (ii) high-efficient thermoelectric power in CuAlO₂ by p-type doping, (iii) half-metallic ferromagnetism in transition-metal-impurity doped CuAlO₂ and ZnO-based diluted magnetic semiconductors, and (iv) CaO, MgO, SrO and BaO based DMS without transition metal impurities. We also discussed the implementation of the self-interaction correction to our materials design method based on the LDA.

ACKNOWLEDGEMENTS This research was partially supported by a Grant-in-Aid for Scientific Research in Priority Areas “Quantum Simulators and QuantumDesign” (No. 17064014) and “Semiconductor Nanospintronics”, a Grand-in-Aid for Scientific Research for young researchers, JST-CREST, NEDO-nanotech, the 21st Century COE and the JSPS core-to-core program “Computational Nano-materials Design”.

REFERENCES

- 1 T. Yamamoto, H. Katayama-Yoshida, Japan. J. Appl. Phys. **36**, L180 (1997)
- 2 T. Yamamoto, H. Katayama-Yoshida, Japan. J. Appl. Phys. **37**, L910 (1998)
- 3 T. Yamamoto, H. Katayama-Yoshida, Japan. J. Appl. Phys. **38**, L166 (1999)
- 4 I. Hamada, H. Katayama-Yoshida, Physica B **376–377**, 808 (2006)
- 5 T. Koyanagi, H. Harima, A. Yanase, H. Katayama-Yoshida, J. Phys. Chem. Solids **64**, 144 (2003)
- 6 K. Sato, H. Katayama-Yoshida, Japan. J. Appl. Phys. **39**, L555 (2000)
- 7 K. Sato, H. Katayama-Yoshida, Japan. J. Appl. Phys. **40**, L334 (2001)
- 8 K. Sato, H. Katayama-Yoshida, Japan. J. Appl. Phys. **40**, L485 (2001)
- 9 K. Sato, H. Katayama-Yoshida, Japan. J. Appl. Phys. **40**, L651 (2001)
- 10 K. Sato, H. Katayama-Yoshida, Semicond. Sci. Technol. **17**, 367 (2002)
- 11 V.A. Dinh, K. Sato, H. Katayama-Yoshida, Solid State Commun. **136**, 1 (2005)
- 12 H. Kizaki, K. Sato, A. Yanase, H. Katayama-Yoshida, Japan. J. Appl. Phys. **44**, L1187 (2005)
- 13 K. Kenmochi, M. Seike, K. Sato, A. Yanase, H. Katayama-Yoshida, Japan. J. Appl. Phys. **43**, L934 (2004)
- 14 K. Kenmochi, V.A. Dinh, K. Sato, A. Yanase, H. Katayama-Yoshida, J. Phys. Soc. Japan **73**, 2952 (2004)
- 15 V.A. Dinh, M. Toyoda, K. Sato, H. Katayama-Yoshida, J. Phys. Soc. Japan **75**, 93705 (2006)
- 16 M. Toyoda, H. Akai, K. Sato, H. Katayama-Yoshida, Physica B **376–377**, 647 (2006)
- 17 H. Katayama-Yoshida, T. Koyanagi, H. Funashima, H. Harima, A. Yanase, Solid State Commun. **126**, 135 (2003)
- 18 H. Funashima, H. Harima, A. Yanase, H. Katayama-Yoshida, presented in 2004 Int. Conf. on Thermoelectrics
- 19 C. Friedel, C.R. Acad. Sci. **77**, 211 (1872)
- 20 H. Kawazoe, M. Yasukawa, H. Hyodo, M. Kurita, H. Yanagi, H. Hosono, Nature **389**, 939 (1997)
- 21 S.B. Zhang, S.H. Wei, A. Zunger, H. Katayama-Yoshida, Phys. Rev. B **57**, 9642 (1998)
- 22 A.F. Ioffe, *Semiconductor Thermoelements and Thermoelectric Cooling* (Infosearch Ltd., London, 1957)
- 23 N.F. Mott, H. Jones, *The Theory of the Properties of Metals and Alloys* (Clarendon, Oxford, 1958)
- 24 H. Akai, P.H. Dederichs, Phys. Rev. B **47**, 8739 (1993)
- 25 <http://sham.phys.sci.osaka-u.ac.jp/kkr>
- 26 K. Sato, P.H. Dederichs, H. Katayama-Yoshida, Europhys. Lett. **61**, 403 (2003)
- 27 K. Sato, P.H. Dederichs, H. Katayama-Yoshida, J. Kudrnovsky, J. Phys.: Condens. Matter **16**, S5491 (2004)
- 28 H. Akai, Phys. Rev. Lett. **81**, 3002 (1998)
- 29 T. Oguchi, K. Terakura, N. Hamada, J. Phys. F **13**, 145 (1983)
- 30 J. Kanamori, J. Phys. Chem. Solids **10**, 87 (1959)
- 31 J.B. Goodenough, Phys. Rev. **100**, 564 (1955)
- 32 A. Zunger, Solid State Phys. **39**, 276 (1986)
- 33 L. Bergqvist, O. Eriksson, J. Kudrnovsky, V. Drchal, P. Korzhavyi, I. Turek, Phys. Rev. Lett. **93**, 137202 (2004)
- 34 K. Sato, W. Schweika, P.H. Dederichs, H. Katayama-Yoshida, Phys. Rev. B **70**, 201202 (2004)
- 35 T. Fukushima, K. Sato, H. Katayama-Yoshida, P.H. Dederichs, Japan. J. Appl. Phys. **43**, L1416 (2004)
- 36 Z. Jin, M. Murakami, T. Fukumura, Y. Matsumoto, A. Ohtomo, M. Kawasaki, H. Koinuma, J. Cryst. Growth **214–215**, 55 (2000)
- 37 S.J. Pearton, C.R. Abernathy, M.E. Overberg, G.T. Thaler, D.P. Norton, N. Theodoropoulou, A.F. Hebard, Y.D. Park, F. Ren, J. Kim, L.A. Boatner, J. Appl. Phys. **93**, 1 (2003)
- 38 H. Saeiki, H. Tabata, T. Kawai, Solid State Commun. **120**, 439 (2001)
- 39 K. Ueda, H. Tabata, T. Kawai, Appl. Phys. Lett. **79**, 988 (2001)
- 40 T. Wakano, N. Fujimura, Y. Morinaga, N. Abe, A. Ashida, T. Ito, Physica C **10**, 260 (2001)
- 41 K. Ando, H. Saito, Z. Jin, T. Fukumura, M. Kawasaki, Y. Matsumoto, H. Koinuma, J. Appl. Phys. **78**, 2700 (2001)
- 42 H. Saito, V. Zayets, S. Yamagata, K. Ando, Phys. Rev. Lett. **90**, 207202 (2004)
- 43 N. Ozaki, N. Nishizawa, K.T. Nam, S. Kuroda, K. Takita, Phys. Stat. Solidi **1**, 957 (2004)
- 44 A. Filippetti, N.A. Spaldin, Phys. Rev. B **67**, 125109 (2003)
- 45 K. Sato, P.H. Dederichs, H. Katayama-Yoshida, Physica B **376–377**, 639 (2006)